A novel finite-volume TVD scheme to overcome non-realizability problem in quadrature-based moment methods

A novel finite-volume TVD scheme to overcome non-realizability problem in quadrature-based moment methods

Mohsen Shiea[a], Antonio Buffo[a,*], Marco Vanni[a], Daniele L. Marchisio[a]

[a] *Dipartimento di Scienza Applicata e Tecnologia, Politecnico di Torino, Corso Duca degli Abruzzi 24, 10129 Torino, Italy*

Abstract

A new finite-volume total variation diminishing (TVD) scheme is proposed for the solution of moment transport equations in quadrature-based moment methods (QBMM). The proposed scheme is capable of preserving important properties of the moments, such as realizability and boundedness. The idea behind the approach is to limit the flux of all the moments at each cell face with the same limiter value. The proposed numerical technique was eventually compared with other realizable schemes developed for the moment transport equations, showing that the method is able to keep the moments realizable and bounded at the same time.

Keywords: Quadrature-based moment methods (QBMM); Moment realizability; Moment boundedness; Population balance equation (PBE); High-resolution scheme; Finite-volume method.

1. Introduction

The evolution in space and time of a population of disperse elements (e.g., droplets, bubbles or particles moving in a continuous fluid) can be described by using an Eulerian approach through the solution of a generalized

*Corresponding author; current mailing address: Dipartimento di Scienza Applicata e Tecnologia, Politecnico di Torino, Corso Duca degli Abruzzi 24, 10129 Torino, Italy; email: antonio.buffo@polito.it; tel.: +390110904758.

population balance equation (GPBE). It is an integro-differential equation written in terms of a number density function (NDF) representing, at every point of the physical space, the number of elements that have a particular state belonging to the so-called phase space, i.e. the space of the properties required to characterize the system under investigation (e.g. element size, velocity, chemical composition, temperature). The Quadrature-Based Moment Methods (QBMM) are proved to be efficient in solving the GPBE, where the transport equations for some moments of the underlying NDF are solved instead of the GPBE [1]. These methods are based on the assumption that the underlying NDF has the form of a multi-dimensional summation of weighted kernel density functions (KDF) centered on the quadrature abscissas, where the quadrature weights and abscissas can be retrieved from the moments by means of the so-called inversion algorithms (such as the Product-Difference (PD) [2] and the Chebyshev [3] algorithms). In most cases, the KDF is a Dirac delta function, especially when a continuous reconstruction of the NDF is not necessary. While these methods are efficient and promising, especially when coupled with Computational Fluid Dynamics (CFD) codes, their practical use encounters inherent difficulties to cope with. One major issue is the realizability or consistency of the transported moment set, meaning that there must exist an underlying number density function (NDF) corresponding to the transported moments. Confining the discussion to the finite-volume method, the most common cause of the non-realizability (also known as numerical moment corruption) lies in the spatial discretization of the transport term of the moment equation, when high-order spatial discretization schemes are used. This problem is often related to the convective term, as in many cases the governing equations have a hyperbolic form. Desjardins et al. [4] demonstrated that the 1$^{\text{st}}$-order scheme guarantees the realizability of the moments, provided the CFL condition is respected. However, this scheme results in highly diffusive solutions, leading sometimes to unacceptable predictions, hence the necessity of adopting high-order schemes. On the other hand, employing high-order finite-volume schemes for independent transport of the moments may cause non-realizability issues [5]. Therefore, the development of a realizable high-order scheme for the solution of moment transport equations is crucial. In this regard, Vikas and co-workers [6] presented the so-called realizable quasi-high-order schemes, based on the evaluation of the moment fluxes at the cell faces using the interpolated abscissas and weights of the quadrature. With this method, the quadrature interpolation is performed by applying 1$^{\text{st}}$-order scheme to the quadrature abscissas and high-order schemes to the quadrature weights. This approach produces less diffusive solutions and guarantees the realizability of the transported moments, provided a criterion on the time step is respected. However, no analysis was conducted on the boundedness property of this approach, which can not be ignored since unbounded predictions are not physically allowed [7]. Kah et al. [8] formulated a 2$^{\text{nd}}$-order kinetic scheme that makes use of the canonical moments to transport the moments indirectly while maintaining them in the moment space. However, the application of their method to simulations with more than four moments involves difficult algebra [9]. Recently, Laurent and co-workers [9] developed a similar approach based on reconstructing the coefficients ζ_k (for its definition refer to [9]) instead of the canonical moments. However, their original ζ_k reconstruction based scheme cannot be applied easily to the unstructured grids and therefore they suggested a simplified version of this scheme that involves division of the cells into three parts as proposed by Berthon [10].

The present work introduces a new technique, called equal-limiter scheme, to overcome the non-realizability problem when 2^{nd}-order TVD (Total Variation Diminishing) schemes are applied to the moment transport equations. The technique is based on using an equal limiter given by the flux-limiter function for all the moments, and it will be shown that it is effective to avoid non-realizable set of moments. Moreover, its application to three-dimensional unstructured grids is straightforward. The paper is organized as follows. First, it will be proved that, in a one-dimensional Riemann problem, the concept of equal-limiter emerges naturally if no source term is included in the moment transport equations. Next, the importance of using an identical limiter given by the limiter function for all the moments will be clarified in a general case by solving local Riemann problem at each cell face and the role of the time step in maintaining the realizability of the moments will be explained. Moreover, the paper shows how this technique can be applied to CFD codes, without any assumption on velocity field or type of mesh grid. In the final part, a comparison between different techniques will be performed by solving moment transport equations in some one- and two-dimensional test cases.

2. TVD scheme for moment transport equation

2.1. Moment transport equation

As previously mentioned, QBMM deal with the solution of the transport equations written in terms of the moments of the NDF, instead of the GPBE itself. The NDF is a complex multi-dimensional functional that depends on the so-called external coordinates, i.e. the position of the elements in the physical space and time, and on the internal coordinates, which are the generic properties associated to each element of the population, such as size, velocity, chemical composition or temperature. When the internal coordinates do not include the velocity of the elements of the disperse phase, the resulting transport equation for the NDF is called Population Balance Equation (PBE) [1]. Although it is possible to apply the proposed numerical scheme to the transport equation for a multivariate set of moments, let us consider a univariate PBE with the size of the elements of the disperse phase, L, as the internal coordinate, for the sake of simplicity and clarity. In this case, the PBE can be written as follows [11]:

$$\frac{\partial f}{\partial t} + \frac{\partial (\mathbf{U} f)}{\partial \mathbf{x}} + \frac{\partial (\dot{L} f)}{\partial L} = h \tag{1}$$

where $f \equiv f(L, \mathbf{x}, t)$ denotes the NDF. In addition, $\mathbf{U} \equiv \mathbf{U}(\mathbf{x}, t)$ is the velocity of the disperse phase, $\dot{L}$ represents the continuous rate of change in the size of elements due to the continuous processes (e.g. mass transfer driven growth) and h introduces the contribution of the discrete events (e.g. aggregation/breakage) into the PBE. It is worth remarking that the velocity of the disperse phase appearing in Eq. (1) does not depend on the size of the elements: such approximation has been made to simplify the following discussion and it is not a limitation of the proposed approach.

By definition, the k^{th}-order moment of f with respect to L is:

$$M^k(\mathbf{x}, t) = \int_0^\infty f(L, \mathbf{x}, t) L^k dL \tag{2}$$

The importance of the moments lies in the fact that lower-order moments are associated to various integral properties of the population. For instance, in this case the 3^{rd}-order moment with respect to L is proportional to the volume fraction of the disperse phase. The above definition can be used to derive moment transport equations from Eq. (1). For the sake of simplicity, from now on we assume a one-dimensional case where the velocity is constant (u) and the contribution of the continuous processes is negligible ($\dot{L} = 0$). The transport equation for the k^{th}-order moment reduces to the following partial differential equation:

$$\frac{\partial M^k}{\partial t} + u \frac{\partial M^k}{\partial x} = \bar{h}^k \tag{3}$$

where $\bar{h}^k$ is the source term changing the k^{th}-order moment due to the discrete events. Generally, this source term is a complex multi-dimensional integral which depends on the NDF itself. QBMM employ the so-called quadrature approximation to express the functional form of the NDF. If we consider only one internal coordinate, it is possible to write a generic integral in the following way and therefore close the moment transport equations:

$$\int_{\Omega_L} f(L) g(L) dL = \sum_{\alpha=1}^{N} w_\alpha g(L_\alpha) \tag{4}$$

where w_α and L_α are the weights and abscissas of the N-node quadrature formula. This means that the NDF is approximated as a summation of delta functions centered on quadrature abscissas:

$$f(L) = \sum_{\alpha=1}^{N} w_\alpha \delta(L - L_\alpha) \tag{5}$$

This method is called Quadrature Method of Moments (QMOM) and it is designed to solve univariate PBE [12]. The weights and abscissas are determined from the transported moments by employing an inversion algorithm (such as PD or Chebyshev algorithms), provided the set of moments is realizable. This is usually referred as the moment problem [13]: in particular, when the support of the NDF is $\Omega_L =]0, +\infty[$ as in this case, it is called finite Stieltjes moment problem. When the support of the NDF is different, i.e. $\Omega_L =]-\infty, +\infty[$ or $\Omega_L =]0, 1[$, we refer to finite Hamburger and finite Hausdorff moment problems respectively. These three different supports result in different constraints on the transported set of moments to ensure its realizability [13, 14]. However, the non-realizability problem is common to all these cases and poses the main challenge in practical applications of QMOM. In the finite-volume method, this can happen particularly during the interpolation of the moments on to the faces to calculate the flux of the moments through faces if high-resolution TVD schemes are employed.

2.2. *Finite-Volume Method*

As mentioned before, the present study focuses on the non-realizability issue in the context of the finite-volume method. The general formulation of the finite-volume method can be found in the specialized literature [15, 16], and therefore is omitted here. Let a single-stage explicit method be adopted to march in time and the source terms be handled using fractional-step approach [15]. In this way, the finite-volume method transforms Eq. (3)

into the following discretized form written for the generic cell i of size Δx in the spatial domain:

$$M_i^{k*} = M_i^k - \frac{\Delta t}{\Delta x}(F_{i+1/2}^k - F_{i-1/2}^k) \tag{6}$$

$$(M_i^k)^{n+1} = M_i^{k*} - \Delta t\ \bar{h}_i^k \tag{7}$$

where M_i^k, M_i^{k*} and $(M_i^k)^{n+1}$ refer to, respectively, the moment value at the current time (t_n), the intermediate value of the fractional-step approach and the moment value at the new time (t_{n+1}) after a time step of Δt. Furthermore, $F_{i-1/2}^k$ and $F_{i+1/2}^k$ denote the numerical flux along the left and right faces of the cell i respectively, each depends on the neighboring cell values at time t_n according to the selected numerical flux function. From now on, the primary focus of the work will be on Eq. (6), particularly the calculation of the flux of the moments at the faces. The effect of the source term will be clarified afterwards.

It is desirable to calculate the fluxes using high-resolution schemes, which are on the basis of slope-limiter methods. These methods use a high-order scheme where the solution is smooth enough, otherwise they switch to a low-order one to prevent non-physical oscillations in the numerical solution [15]. In this way, the solution exhibits higher order of accuracy, comparing to 1$^{\text{st}}$-order solution, without losing the boundedness. Using Lax-Wendroff as the high-order scheme and upwind as the low-order one will form the so-called flux-limiter methods with the following numerical flux functions [15]:

$$F_{i-1/2}^k = u^- M_i^k + u^+ M_{i-1}^k + \frac{1}{2}|u|\left(1 - \frac{|u|\Delta t}{\Delta x}\right)\phi(\theta_{i-1/2}^k)\Delta M_{i-1/2}^k \tag{8}$$

$$F_{i+1/2}^k = u^- M_{i+1}^k + u^+ M_i^k + \frac{1}{2}|u|\left(1 - \frac{|u|\Delta t}{\Delta x}\right)\phi(\theta_{i+1/2}^k)\Delta M_{i+1/2}^k \tag{9}$$

where

$$u^+ = \frac{1}{2}(u + |u|) \quad \text{and} \quad u^- = \frac{1}{2}(u - |u|) \tag{10}$$

In addition, $\Delta M^k_{i-1/2}$ and $\Delta M^k_{i+1/2}$ are respectively the jumps across the left and right faces, defined following the below convention:

$$\Delta M^k_{i-1/2} = M^k_i - M^k_{i-1} \tag{11}$$

The flux-limiter ϕ is a function of the smoothness of M^k at the face ($\theta^k_{i\pm1/2}$). The smoothness is commonly defined as follows [15]:

$$\theta^k_{i-1/2} = \frac{\Delta M^k_{I-1/2}}{\Delta M^k_{i-1/2}} \quad \text{with} \quad I = \begin{cases} i-1 & \text{if } u > 0 \\ i+1 & \text{if } u < 0 \end{cases} \tag{12}$$

A variety of flux-limiter functions are available in the literature such as min-mod [17] and van Leer [18].

Substituting the numerical fluxes in Eq. (6) yields the following discretized equation:

$$\begin{aligned} M^{k*}_i = M^k_i &- \frac{\Delta t}{\Delta x} u^+ (M^k_i - M^k_{i-1}) - \frac{\Delta t}{\Delta x} u^- (M^k_{i+1} - M^k_i) \\ &- \frac{1}{2}\frac{|u|\Delta t}{\Delta x}\left(1 - \frac{|u|\Delta t}{\Delta x}\right)\left[\phi(\theta^k_{i+1/2})\Delta M^k_{i+1/2} - \phi(\theta^k_{i-1/2})\Delta M^k_{i-1/2}\right] \end{aligned} \tag{13}$$

3. The Concept of Equal-Limiter

The flux-limiter methods were developed to address the issue of boundedness that occurs in the case of employing high-order schemes to solve hyperbolic problems. One would ideally desire to use these methods for the solution of the moment transport equations, particularly when the 1st-order accuracy is not sufficient to describe the behavior of the system under study. However, in general, the non-realizability problem hinders their direct practice in solving the moments transport equations. In this section, it is shown that this limitation can be overcome by selecting an equal limiter for all the moments.

The starting point is to show that the idea of equal-limiter emerges in the case of employing 2[nd]-order TVD schemes for the pure moment advection with no source term ($(M_i^k)^{n+1} = M_i^{k*}$) in a Riemann problem example. It will be also shown that in this case the moments remain realizable. Then, the discussion will continue to highlight the advantage of employing equal-limiter in a more general context, where the effect of aggregation and breakage will be also taken into account.

The argument begins with rewriting Eq. (13) for the case $u > 0$ without loss of generality[1]:

$$\begin{aligned}(M_i^k)^{n+1} = M_i^k - \nu(M_i^k - M_{i-1}^k) \\ - \frac{1}{2}\nu(1-\nu)\left[\phi(\theta_{i+1/2}^k)\Delta M_{i+1/2}^k - \phi(\theta_{i-1/2}^k)\Delta M_{i-1/2}^k\right]\end{aligned} \tag{14}$$

where $\nu = u\Delta t/\Delta x$ is the Courant number. The smoothness at the left and right faces are written as follows Eq. (12):

$$\theta_{i-1/2}^k = \frac{M_{i-1}^k - M_{i-2}^k}{M_i^k - M_{i-1}^k} \quad \text{and} \quad \theta_{i+1/2}^k = \frac{M_i^k - M_{i-1}^k}{M_{i+1}^k - M_i^k} \tag{15}$$

Now let us consider a Riemann problem example with the following initial

[1] The case $u < 0$ can be formulated similarly and leads to the same conclusions

data:

$$M^k(x,0) = \overset{\circ}{M}{}^k = \begin{cases} \overset{\circ}{M}{}_l^k & \text{if } x < 0 \\ \overset{\circ}{M}{}_r^k & \text{if } x > 0 \end{cases} \tag{16}$$

where $\overset{\circ}{M}{}_l^k$ and $\overset{\circ}{M}{}_r^k$ are obtained from the initial left and right NDFs, $\overset{\circ}{f}_l$ and $\overset{\circ}{f}_r$, and consequently constitute two realizable sets of moments. It is postulated that the numerical solution of the k^{th}-order moment at any generic cell i and any time step t_n, including the zero time, can be expressed as:

$$M_i^k = \overset{\circ}{M}{}_r^k - a_i^n(\overset{\circ}{M}{}_r^k - \overset{\circ}{M}{}_l^k) \quad , \quad 0 \le a_i^n \le 1 \tag{17}$$

where a_i^n is a constant that changes with the cell index i and the time step but not due to the moment order or value. In other words, this constant is the same for all the moments of a given cell at each time step. It is worth mentioning that the initial data (Eq. (16)) corresponds to $a_i^0 = 1$ for $x_i < 0$ and $a_i^0 = 0$ for $x_i > 0$. Next step is to substitute Eq. (17) in Eq. (14), which after simplifications yields the following:

$$\begin{aligned}(M_i^k)^{n+1} &= \overset{\circ}{M}{}_r^k - a_i^n(\overset{\circ}{M}{}_r^k - \overset{\circ}{M}{}_l^k) + \nu(a_i^n - a_{i-1}^n)(\overset{\circ}{M}{}_r^k - \overset{\circ}{M}{}_l^k) \\ &\quad + \frac{1}{2}\nu(1-\nu)\Bigg[\phi\left(\frac{a_i^n - a_{i-1}^n}{a_{i+1}^n - a_i^n}\right)(a_{i+1}^n - a_i^n) \\ &\quad - \phi\left(\frac{a_{i-1}^n - a_{i-2}^n}{a_i^n - a_{i-1}^n}\right)(a_i^n - a_{i-1}^n)\Bigg](\overset{\circ}{M}{}_r^k - \overset{\circ}{M}{}_l^k) \\ &= \overset{\circ}{M}{}_r^k - a_i^{n+1}(\overset{\circ}{M}{}_r^k - \overset{\circ}{M}{}_l^k)\end{aligned} \tag{18}$$

and a_i^{n+1} collects several coefficients that do not depend on the moment values:

$$
\begin{aligned}
a_i^{n+1} = a_i^n - \nu(a_i^n - a_{i-1}^n) \\
- \frac{1}{2}\nu(1-\nu)\left[\phi\left(\frac{a_i^n - a_{i-1}^n}{a_{i+1}^n - a_i^n}\right)(a_{i+1}^n - a_i^n)\right. \\
\left. - \phi\left(\frac{a_{i-1}^n - a_{i-2}^n}{a_i^n - a_{i-1}^n}\right)(a_i^n - a_{i-1}^n)\right]
\end{aligned}
\tag{19}
$$

Equation (19) has the same structure of Eq. (14), therefore, it appears that a_i^n is the solution of an advection equation for the variable a obtained by the 2nd-order TVD finite-volume scheme. As a consequence, it is guaranteed that a_i^{n+1} remains bounded to the values of the previous time step, i.e. between 0 and 1. Now it can be concluded that the postulated solution at time step t_n is also valid at the next time step t_{n+1}:

$$
(M_i^k)^{n+1} = \mathring{M}_r^k - a_i^{n+1}(\mathring{M}_r^k - \mathring{M}_l^k) \quad , \quad 0 \le a_i^{n+1} \le 1 \tag{20}
$$

As mentioned before, the initial data (Eq. (16)) can be expressed by Eq. (17), therefore, the postulated solution is indeed the solution of Eq. (14) at any time step with the initial data defined by Eq. (16). Moreover, it can be proved that the solution guarantees the realizability of the moments at any time step if the initial set is realizable. To proceed with the proof, the following notation is used for representing the set of moments:

$$
\mathbf{W} = \begin{bmatrix} M^0 & M^1 & ... & M^{2N-1} \end{bmatrix}^T \tag{21}
$$

It is worth reiterating that N is the number of quadrature nodes. The set of moments can be defined as follows:

$$
\mathbf{W} = \int_0^\infty f(L)\mathbf{q}(L)dL \tag{22}
$$

where $\mathbf{q}(L) = [L^0 \quad L^1 \quad ... \quad L^{2N-1}]^T$.

Equation (20) can be written for the set of moments by using the notation introduced in Eq. (21):

$$\mathbf{W}_i^{n+1} = \mathbf{W}_r - a_i^{n+1}(\mathbf{W}_r - \mathbf{W}_l) \tag{23}$$

It should be emphasized that Eq. (23) is derived based on the fact that a_i^{n+1} is identical for all the moments. The proof follows by substituting Eq. (22) in Eq. (23) and performing some manipulations:

$$\int_0^\infty f_i^{n+1}\mathbf{q}(L)dL = \int_0^\infty [(1 - a_i^{n+1})\mathring{f}_r + a_i^{n+1}\mathring{f}_l]\mathbf{q}(L)dL \tag{24}$$

or

$$f_i^{n+1} = (1 - a_i^{n+1})\mathring{f}_r + a_i^{n+1}\mathring{f}_l \tag{25}$$

The above equation guarantees the non-negativity of the f_i^{n+1} because both $\mathring{f}_r$ and $\mathring{f}_l$ are defined to be non-negative NDFs and $0 \leq a_i^{n+1} \leq 1$. Consequently, the moment set of cell i at time step t_{n+1} is realizable, see [4].

Returning back to the equal-limiter concept, it was previously highlighted that an identical a_i^{n+1} for all the moments is essential to keep the moment set realizable in a Riemann problem example. The identical a_i^{n+1} originates, in turn, from the equal limiters calculated at the left and right faces (i.e., Eq. (18)):

$$\phi(\theta_{i-1/2}^k) = \phi\left(\frac{a_{i-1}^n - a_{i-2}^n}{a_i^n - a_{i-1}^n}\right) \quad \text{and} \quad \phi(\theta_{i+1/2}^k) = \phi\left(\frac{a_i^n - a_{i-1}^n}{a_{i+1}^n - a_i^n}\right). \tag{26}$$

When source terms are present, the limiters are not generally identical for all the moments, because in this case the smoothness of the moments may change differently and this may cause the non-realizability of the transported moment set. This suggests to find a technique to employ an identical limiter in the calculation of the moment fluxes at the faces.

Again Eq. (13) is rewritten for the case of $u > 0$ (here a local Riemann problem is solved at each face of cell i):

$$\begin{aligned} M_i^{k*} &= M_i^k - \nu(M_i^k - M_{i-1}^k) \\ &\quad - \frac{1}{2}\nu(1-\nu)[\phi(\theta_{i+1/2}^k)\Delta M_{i+1/2}^k - \phi(\theta_{i-1/2}^k)\Delta M_{i-1/2}^k] \end{aligned} \tag{27}$$

which can simply be expressed as follows by collecting the terms containing the moment of cells $i-1$, i and $i+1$:

$$M_i^{k*} = B_i^k M_{i-1}^k + C_i^k M_i^k - D_i^k M_{i+1}^k \tag{28}$$

with

$$\begin{aligned} B_i^k &= \nu - \frac{1}{2}\nu(1-\nu)\phi(\theta_{i-1/2}^k) \\ C_i^k &= 1 - \nu + \frac{1}{2}\nu(1-\nu)[\phi(\theta_{i+1/2}^k) + \phi(\theta_{i-1/2}^k)] \\ D_i^k &= \frac{1}{2}\nu(1-\nu)\phi(\theta_{i+1/2}^k) \end{aligned} \tag{29}$$

Writing Eq. (28) for the set of moments of order $k = 1, 2, ..., 2N-1$ yields:

$$\begin{pmatrix} M_i^{0*} \\ M_i^{1*} \\ \vdots \\ M_i^{2N-1*} \end{pmatrix} = \underbrace{\begin{pmatrix} B_i^0 M_{i-1}^0 \\ B_i^1 M_{i-1}^1 \\ \vdots \\ B_i^{2N-1} M_{i-1}^{2N-1} \end{pmatrix}}_{\text{set i-1}} + \underbrace{\begin{pmatrix} C_i^0 M_i^0 \\ C_i^1 M_i^1 \\ \vdots \\ C_i^{2N-1} M_i^{2N-1} \end{pmatrix}}_{\text{set i}} - \underbrace{\begin{pmatrix} D_i^0 M_{i+1}^0 \\ D_i^1 M_{i+1}^1 \\ \vdots \\ D_i^{2N-1} M_{i+1}^{2N-1} \end{pmatrix}}_{\text{set i+1}} \tag{30}$$

The three sets of moments in Eq. (30) can easily become non-realizable because, in general, the coefficients B_i^k as well as C_i^k and D_i^k might differ from one moment to another (belonging to the same moment set) as a consequence of unequal limiters. Marchisio and Fox [1] showed that a small change in just one moment can make a consistent set of moments non-realizable. On the other hand, if identical limiters are selected to estimate the fluxes of all the moments at the left and right faces, Eq. (30) can be written as follows:

$$\int_0^\infty f_i^* \mathbf{q}(L) dL = \int_0^\infty (B_i f_{i-1} + C_i f_i - D_i f_{i+1}) \mathbf{q}(L) dL \tag{31}$$

or

$$f_i^* = B_i f_{i-1} + C_i f_i - D_i f_{i+1} \tag{32}$$

where B_i as well as C_i and D_i are defined below by choosing an equal limiter at the left face, $\phi(\theta_{i-1/2})$, and one at the right face, $\phi(\theta_{i+1/2})$, for all the moments:

$$\begin{aligned} B_i &= \nu - \frac{1}{2}\nu(1-\nu)\phi(\theta_{i-1/2}) \\ C_i &= 1 - \nu + \frac{1}{2}\nu(1-\nu)[\phi(\theta_{i+1/2}) + \phi(\theta_{i-1/2})] \\ D_i &= \frac{1}{2}\nu(1-\nu)\phi(\theta_{i+1/2}) \end{aligned} \tag{33}$$

It should be noted that there is still no proof for the moment realizability in the case of employing equal limiters when source terms in the moment transport equation are present, because the last term in Eq. (32) is negative [4] [6]. However, the contribution of the negative term can be kept small enough through adjusting the time step since the coefficient D_i diminishes as the time step is reduced to zero. In other words, the non-realizability problem can be prevented by adjusting the time step, whereas it can arise easily regardless of the time step if the limiters are calculated independently. One should be careful when the moment sets lie on the boundary of the moment space. In such case, the underlying number density functions are indeed some point distributions, i.e summation of some weighted delta functions. Therefore, if the moment sets in Eq. (30) are near or on the boundary of the moment space, reduction of the time step cannot resolve the realizability issue since the supports of the corresponding underlying number density functions in Eq. (32) may hardly match each other. A possible remedy can be adopting the 1-D adaptive quadrature technique proposed by Yuan and co-workers [19]. By this technique, the maximum number of quadrature nodes is selected in such a way that the moments required to calculate the quadrature weights and abscissas form a set which is located in the interior of the moment space. It is noteworthy that the local reduction of the number of quadrature nodes is not a problem for the equal-limiter scheme, in contrast to the quasi-high-order scheme, since the variables to be interpolated are the moments and not the quadrature abscissas and weights.

The final point to be addressed is the choice of an equal flux-limiter at each face. In fact, the constraint on the boundedness of the solution narrows the choice of the equal flux-limiter. As mentioned before, the 2^{nd}-order TVD schemes have this notable feature of preserving the solution bounded. It is extremely useful for the QMOM since the low-order moments are proportional to physical properties that are bounded in nature, such as mean size, surface area or volume fraction. Harten [20] established the sufficient criteria for a scheme to be TVD, which provide constraints on the flux-limiter functions:

$$\phi(\theta) = 0 \quad \text{if} \quad \theta < 0 \qquad \text{and} \qquad 0 \leq \phi(\theta) \leq \min(2\theta, 2) \quad \text{if} \quad \theta \geq 0 \quad (34)$$

Fig. 1 represents these constraints graphically (shaded area) following the work of Sweby [21]. Moreover, it depicts the 2nd-order region proposed by Sweby [21] (hatched area) within which the flux-limiter functions lie. Two such examples are shown by the solid line (minmod limiter [17]) and the dashed line (van Leer limiter [18]).

The flux-limiter functions in the literature share the common feature of being non-decreasing functions of θ. Using this feature, it is simple to show that the smallest flux-limiter among all the limiters of the moments is an obvious choice that guarantees the boundedness of all the moments. The flux-limiters calculated independently by a general limiter function at a given face, e, can be represented as $\phi(\theta_e^k)$ with $k = 0, 1, ..., 2N-1$. These limiters respect the conditions expressed in Eq. (34):

$$\phi(\theta_e^k) = 0 \quad \text{if} \quad \theta_e^k < 0 \qquad \text{and} \qquad 0 \leq \phi(\theta_e^k) \leq \min(2\theta_e^k, 2) \quad \text{if} \quad \theta_e^k \geq 0 \quad (35)$$

Suppose that $\phi_e^{\min}$ denotes the limiter with the minimum value:

$$\phi_e^{\min} = \phi(\theta_e^m) \leq \phi(\theta_e^k) \quad \text{for} \quad k = 0, 1, ..., 2N-1 \quad (36)$$

where

$$\theta_e^m \in \{\theta_e^k \mid k \in \{0, 1, ..., 2N-1\}\} \quad (37)$$

and since the flux-limiter functions are non-decreasing:

$$\theta_e^m \leq \theta_e^k \quad \text{for} \quad k = 0, 1, ..., 2N-1 \quad (38)$$

On the other hand, the upper boundary of the TVD region shown in Eq. (35), $\min(2\theta_e^k, 2)$, is a non-decreasing function, therefore:

$$\min(2\theta_e^m, 2) \leq \min(2\theta_e^k, 2) \quad \text{for} \quad k = 0, 1, ..., 2N-1 \tag{39}$$

since $\phi_e^{\min}$ respects the conditions specified in Eq. (35), it can be concluded that:

$$0 \leq \phi_e^{\min} \leq \min(2\theta_e^k, 2) \quad \text{for} \quad k = 0, 1, ..., 2N-1 \tag{40}$$

in other words, $\phi_e^{\min}$ falls always in the TVD region specified in Fig. 1 for all the moments. As a result, the moments remain bounded using this limiter, following the proof given by Harten [20].

It should be mentioned that, in general, the minimum limiter can fall outside the 2nd-order region of Sweby for some moments, hence resulting in solutions with accuracy of lower order. Nevertheless, the numerical results reported in the next section show remarkable improvements in comparison to the 1st-order solutions. More importantly, the results indicate a significant advantage of the proposed scheme over the realizable high-order scheme of Vikas et al. [6] since it is able to produce bounded solutions.

4. Application to CFD Codes

This section focuses on the application of the equal-limiter scheme to CFD codes, which is indeed our ultimate goal of introducing this scheme. For this purpose, the following three-dimensional conservative transport equation is considered for the k^{th}-order moment:

$$\frac{\partial M^k}{\partial t} + \frac{\partial}{\partial \mathbf{x}} \cdot (\mathbf{u} M^k) = 0 \tag{41}$$

The source term is not included since the focus is only on the advection of the moments. In the context of finite volume methods, Eq. (41) is integrated over the volume of each computational cell and then the integral of the convective term over the volume of each cell is replaced with the net flux of the moment through the faces of that cell (Gauss's theorem). Therefore, the following semi-discretized equation is obtained for a generic cell i [16]:

$$\frac{\mathrm{d}M_i^k}{\mathrm{d}t} + \frac{1}{\Delta V_i}\sum_e (\mathbf{u}_e \cdot \hat{\mathbf{n}}_e) S_e M_e^k = 0 \tag{42}$$

where M_e^k and $\mathbf{u}_e$ are the moment of order k and the velocity at a generic face e of cell i respectively. In addition, $\hat{\mathbf{n}}_e$ and S_e denote respectively the outward unit normal vector and the surface area of face e and ΔV_i is the volume of the cell i. The transient term in Eq. (42) is not discretized for the reason that becomes clear later. In CFD codes, the flux of the velocity field at the cell faces, i.e. $(\mathbf{u}_e \cdot \hat{\mathbf{n}}_e)S_e$, is generally known. However, the value of the moments at the faces (M_e^k) is not available and should be interpolated from the values at the centers of neighbouring cells.

The implementation of high-resolution TVD schemes in CFD codes is usually on the basis of central-difference scheme, of which the anti-diffusive contribution is limited to prevent oscillations in the solution [22]:

$$M_e^k = \underbrace{M_{\mathrm{U}}^k}_{\text{upwind}} + \phi(\theta_e^k)\,\underbrace{\lambda_e(M_{\mathrm{D}}^k - M_{\mathrm{U}}^k)}_{\text{anti-diffusive part}} \tag{43}$$

where M_{U}^k and M_{D}^k refer to the values of the moment of order k at the centers of the upwind and downwind cell neighbours of the face e respectively. The selection of the upwind and downwind cells is based on the direction of the velocity field at face e, which is the same for all the moments. In addition, the coefficient λ_e takes a positive constant value between 0 and 0.5, which depends on the distances between the center of face e and the centers of the two neighbouring cells. The advantage of employing an identical limiter can be illustrated by rearranging Eq. (43) and writing it for a set of $2N-1$ moments as follows:

$$\underbrace{\begin{pmatrix} M_e^0 \\ M_e^1 \\ \vdots \\ M_e^{2N-1} \end{pmatrix}}_{\text{set e}} = \underbrace{\begin{pmatrix} \left[1-\lambda_e\phi(\theta_e^0)\right] M_{\mathrm{U}}^0 \\ \left[1-\lambda_e\phi(\theta_e^1)\right] M_{\mathrm{U}}^1 \\ \vdots \\ \left[1-\lambda_e\phi(\theta_e^{2N-1})\right] M_{\mathrm{U}}^{2N-1} \end{pmatrix}}_{\text{set U}} + \underbrace{\begin{pmatrix} \lambda_e\phi(\theta_e^0) M_{\mathrm{D}}^0 \\ \lambda_e\phi(\theta_e^1) M_{\mathrm{D}}^1 \\ \vdots \\ \lambda_e\phi(\theta_e^{2N-1}) M_{\mathrm{D}}^{2N-1} \end{pmatrix}}_{\text{set D}} \tag{44}$$

In general, the limiters for different moments, $\phi(\theta_e^0), \phi(\theta_e^1), \ldots, \phi(\theta_e^{2N-1})$ are not the same. Therefore, the moment sets "U" and "D" can easily become non-realizable, leading to the non-realizable set of interpolated moments at face e. However, selecting an identical limiter, let it be $\phi_e^{\min}$, guarantees the realizability of the interpolated moment set e, as long as the moment sets "U" and "D" are realizable:

$$\underbrace{\begin{pmatrix} M_e^0 \\ M_e^1 \\ \vdots \\ M_e^{2N-1} \end{pmatrix}}_{\text{set e}} = (1-\lambda_e\phi_e^{\min}) \underbrace{\begin{pmatrix} M_{\mathrm{U}}^0 \\ M_{\mathrm{U}}^1 \\ \vdots \\ M_{\mathrm{U}}^{2N-1} \end{pmatrix}}_{\text{set U}} + \lambda_e\phi_e^{\min} \underbrace{\begin{pmatrix} M_{\mathrm{D}}^0 \\ M_{\mathrm{D}}^1 \\ \vdots \\ M_{\mathrm{D}}^{2N-1} \end{pmatrix}}_{\text{set D}} \tag{45}$$

It is worth reiterating that the value of limiter $\phi_e^{\min}$ is between 0 and 2. Moreover, the moment sets "U" and "D" belong to the previous time step if an explicit method is used to advance in time, and therefore they are realizable.

It should be noted that the realizability of the interpolated moments on the faces does not ensure the realizability of the calculated moments at the new time step. To elaborate, let the transient term in Eq. (42) be integrated using an explicit Euler scheme [16] and then write the fully-discretized equation for the set of $2N-1$ moments:

$$\mathbf{W}_i^{n+1} = \mathbf{W}_i^n - \frac{\Delta t}{\Delta V_i} \sum_e (\mathbf{u}_e^n \cdot \hat{\mathbf{n}}_e) S_e \mathbf{W}_e^n \tag{46}$$

The use of an identical limiter for all the moments guarantees that the moment set $\mathbf{W}_e^n$ be realizable, and therefore an underlying number density function (f_e^n) can be associated to it. This allows writing Eq. (46) as:

$$f_i^{n+1} = f_i^n - \frac{\Delta t}{\Delta V_i} \sum_e (\mathbf{u}_e^n \cdot \hat{\mathbf{n}}_e) S_e f_e^n \tag{47}$$

The summation in the above equation can be separated into two contributions of in-going and out-going fluxes:

$$f_i^{n+1} = f_i^n - \underbrace{\frac{\Delta t}{\Delta V_i} \sum_e \min[(\mathbf{u}_e^n \cdot \hat{\mathbf{n}}_e), 0] S_e f_e^n}_{\text{in-going fluxes}} - \underbrace{\frac{\Delta t}{\Delta V_i} \sum_e \max[(\mathbf{u}_e^n \cdot \hat{\mathbf{n}}_e), 0] S_e f_e^n}_{\text{out-going fluxes}} \tag{48}$$

The in-going fluxes have positive sign and cannot rise the realizability issue, whereas, the outgoing fluxes have negative sign and can cause realizability issue, i.e. negativity of f_i^{n+1}. However, the out-going fluxes can be still decomposed into two separate upwind and downwind contributions corresponding to the upwind and downwind neighbouring cells of the corresponding faces. It is noteworthy that the upwind cell of these faces indeed coincides with cell

i since the flux at these faces is out-going. Thus, the first and third terms of the RHS of Eq. (48) can be written as follows:

$$\left(1-(1-\lambda_e\phi_e^{\min})\frac{\Delta t}{\Delta V_i}\sum_e \max[(\mathbf{u}_e^n\cdot\hat{\mathbf{n}}_e),0]S_e\right)f_i^n \\ -(1-\lambda_e\phi_e^{\min})\frac{\Delta t}{\Delta V_i}\sum_e \max[(\mathbf{u}_e^n\cdot\hat{\mathbf{n}}_e),0]S_e f_{D_e}^n \quad (49)$$

where $f_{D_e}^n$ denotes the (downwind) neighbouring cell separated by face e from cell i. As can be seen, the entire contribution of the cell i is positive as long as the coefficient behind f_i^n is positive, leading to the following CFL-like condition:

$$\frac{\Delta t}{\Delta V_i}\sum_e \max[(\mathbf{u}_e^n\cdot\hat{\mathbf{n}}_e),0]S_e<1 \quad (50)$$

Therefore, the only remaining negative contributions are due to the information (distributions) of the downwind cells (with respect to cell i) that propagates back into cell i, which is the characteristic of high-order schemes. These negative contributions can generally lead to the non-realizability issue, i.e. negativity of f_i^{n+1}. However, similar to the previous discussion done for one-dimensional constant-velocity cases, the negative contributions can be kept small (in comparison to the contribution of f_i^n) by controlling the time step. It is noteworthy that this technique may fail as the moment sets are near/at the boundary of the moment space, as explained before.

Returning back to the time-integration of the transient term in Eq. (42), it should be noted that one notable advantage of the equal-limiter scheme is the possibility of using implicit time-integration for the advection of the moments. This is due the fact that the equal-limiter scheme interpolates the moments directly, whereas, for instance, the quasi-high-order scheme is normally implemented using explicit time-integration schemes. This aspect is particularly important when the solution of the population balance equation is incorporated into a CFD solver, since the implicit time-integration schemes are commonly adopted in these codes.

Lastly, the proposed technique is very simple from the computational point of view and can be easily implemented in three-dimensional CFD solvers. The only additional steps are comparing the limiter values calculated for the moments at each face and then replacing them with the smallest one at the corresponding face.

5. Numerical Examples

This section evaluates the performance of the proposed technique for the advection of moments in two different parts. The first one is focused on comparing the predictions obtained by different schemes for the advection of the moments in a mono-dimensional constant-velocity problem. The second part evaluates the performance of the schemes by solving the moment transport equations coupled with the CFD simulation of a two-dimensional transient lid-driven cavity flow.

5.1. One-dimensional advection with constant-velocity

This part employs the equal-limiter scheme for the advection of moments in spatially mono-dimensional problems with the disperse particle size as the only internal coordinate of the PBE. The first example deals with the pure advection of the moments without any source term, while the next examples includes the aggregation/breakage source terms in the moment transport equations. The results are compared with those obtained via a 1^{st}-order scheme and the realizable high-order scheme (or quasi-2^{nd}-order scheme) by Vikas et al. [6]. In addition, the analytical solution is reported whenever it is available.

All the cases use 3-node quadrature to approximate the NDF. This number of nodes requires to track the first 6 moments with respect to the particle size, $M^0, M^1, ..., M^5$. The calculation of the weights and abscissas of the quadrature is done by using the Chebyshev algorithm. The spatial problems are defined over the spatial domain $[0, 1]$, which is discretized to cells of identical size $\Delta x = 0.01$. The fluxes at the faces are calculated using high-resolution limited-flux methods. The limiters, in turn, are computed using the minmod function, as it was also used by Vikas et al [6]. Two ghost cells at the left side of the domain and one ghost cell at the right side are considered to cope with the three-cell stencil required by the high-resolution schemes. The advection velocity, u, is set to 1.0 and Δt is calculated by fixing the CFL condition equal to 0.5. The following solution procedure is used to advance in time starting from the initial data, which is based on the explicit fractional-step method for time integration:

1. Initialize the moments in the interior domain.
2. Apply the boundary conditions at the two left ghost cells.
3. Calculate the limiters for all the moments at each face.
4. Find the minimum limiter at each face.
5. Calculate the flux of the moments using the minimum limiter at each face.

6. Compute the intermediate values of the moments at each interior cell using the fluxes at the corresponding left and right faces after a time step equal to Δt.

7. Find the weights and the abscissas of the quadrature at each interior cell using the intermediate values of the moments.

8. Calculate the source contributions at each interior cell using the corresponding quadrature approximation of the NDF.

9. Advance the intermediate values of the moments at each interior cell by one time step Δt using the calculated source terms.

10. Apply the boundary condition at the right ghost cell using zero-order extrapolation from the last interior cell of the domain.

11. Repeat steps 3 to 10 until obtaining the solution at the desired time.

Steps 8 and 9 (fractional-step approach) are obviously required only if the source terms are present. In this work, the source terms are treated by a single-stage method as explained in steps 8 and 9. However, these steps can be modified to use a two-stage method, leading to higher accuracy for the fractional-step approach as explained by LeVeque [15]. It should be emphasized that this suggestion concerns the application of two-stage methods only for updating the intermediate moments by the source terms. Therefore, no realizability issue is generally expected in case of using two-stage methods instead of one-stage method only to treat the source terms, provided that the intermediate moments after the advection are realizable. Furthermore, step 7 is done even in the case without source term to check the realizability of the moments.

More details on the problem settings are presented for each case separately.

5.1.1. Pure advection of the moments

The first example is the one-dimensional pure advection of the moments, i.e. no source term, with the following initial and boundary conditions:

$$
\begin{aligned}
&IC: \quad M^k(x_i, 0) = \overset{\circ}{M}^k \qquad \text{for} \quad i = 0, 1, 2, ..., p \\
&BC \text{ (ghost cells)}: \quad \begin{cases} M^k(x_{-1}, t_n) = M^k(x_{-2}, t_n) = M_b^k \\ M^k(x_{p+1}, t_n) = M^k(x_p, t_n) \end{cases}
\end{aligned} \tag{51}
$$

where the interior cells are numbered from 0 to p. The initial conditions $\overset{\circ}{M}^k$ and the boundary conditions M_b^k are two sets of scaled moments having the shape of different log-normal distributions, $\overset{\circ}{Y}$ and Y_b. The parameters of the distributions, i.e. the mean and the standard deviation of the corresponding normal distributions, are respectively $(\overset{\circ}{\mu}, \overset{\circ}{\sigma}) = (\ln(0.008), 0.22)$ and $(\mu_b, \sigma_b) = (\ln(0.005), 0.2)$. Furthermore, the zero-order moments are $\overset{\circ}{M}^0 = 20000$ and $M_b^0 = 800000$ respectively. It should be noted that the two log-normal distributions have different parameters to avoid their quadrature approximations having the same abscissas. Otherwise, the interpolated abscissas on the faces are identical to those of the cells regardless of the employed scheme. Then, it is trivial to show that, in this special case, the quasi-2$^{\text{nd}}$-order scheme proposed by Vikas et al. [6] is essentially the same as applying 2$^{\text{nd}}$-order scheme directly to the moments.

Figure 2 compares the results obtained from 1$^{\text{st}}$-order scheme, quasi-2$^{\text{nd}}$-

order scheme and the proposed equal-limiter scheme. Furthermore, the analytical solution is plotted in Fig. 2 to provide a benchmark. It is pointless to report the results by the standard 2$^{\mathrm{nd}}$-order TVD scheme since, as proved before, the corresponding results would be identical to those obtained by the equal-limiter scheme. As expected, the solution given by the 1$^{\mathrm{st}}$-order scheme is very diffusive. The quasi-2$^{\mathrm{nd}}$-order scheme improves the accuracy of the results by applying 2$^{\mathrm{nd}}$-order scheme to the weights. However, the moments do not remain bounded simply because applying a TVD scheme to the weights does not guarantee the boundedness of the transported moments, hence appearance of the non-physical oscillations in the solutions. The least oscillations belong to the moment of order zero as expected, since it is simply equivalent to the sum of the weights, the variable to which the TVD scheme is applied in the quasi-2$^{\mathrm{nd}}$-order scheme. The oscillations become more obvious as the moment order increases. It should be noted that, according to our tests, the oscillations may increase or vanish depending on the characteristics of the underlying NDFs. The best predictions belong to the equal-limiter scheme which is indeed the full 2$^{\mathrm{nd}}$-order TVD scheme since this numerical example is the same as the pure advection Riemann problem studied in Section 3. Consequently, the predictions are bounded and without any oscillation.

5.1.2. Moment advection with source term

The next examples deal with a more practical application. The moments of a particle size distribution are introduced and advected in the domain while they are subject to local changes due the effect of the aggregation/breakage of the particles. The initial and boundary conditions are the same as the case of pure advection (see Eq. (51)). In the following, two cases are presented in which the aggregation and breakage are considered separately. Both aggregation and breakage are modeled by assuming a constant kernel. For the case of breakage, the daughter size distribution is expressed by assuming symmetric fragmentation of the particles [23]. The reasoning behind these simplistic assumptions is the possibility of obtaining analytical solutions for the moments of the NDF.

Constant aggregation kernel. In this case, the source term in Eq. (7) is calculated as follows [23]:

$$h_i^k = \frac{1}{2}\sum_{\alpha=1}^{3} w_{i,\alpha} \sum_{\beta=1}^{3} w_{i,\beta}(L_{i,\alpha}^3 + L_{i,\beta}^3)^{k/3} K_a - \sum_{\alpha=1}^{3} L_{i,\alpha}^k w_{i,\alpha} \sum_{\beta=1}^{3} w_{i,\beta} K_a \quad (52)$$

where $K_a = 10^{-5}$ $(m^3 \cdot s^{-1})$ is the aggregation kernel.

The solutions obtained by the studied schemes are shown in Fig. 3. As can be seen, both quasi-2$^{\text{nd}}$-order and equal-limiter schemes improve the accuracy of the results with respect to the 1$^{\text{st}}$-order scheme. It is notable that, despite employing the minimum limiter, the equal-limiter scheme produces almost comparable results to those of the quasi-2$^{\text{nd}}$-order scheme. Moreover, the solutions of M^3 indicate that only 1$^{\text{st}}$-order and equal-limiter schemes are bounded, as expected. Instead, a slight degree of overshoot and undershoot exists in the solution of the quasi-2$^{\text{nd}}$-order scheme. The appearance of these spurious oscillations is certainly due to the numerics as both aggregation and breakage of the particles have no effect on the moment of order three with respect to the particle size. Although no analytical solution is available for M^5, some degree of overshoot and undershoot can be observed visually in the solution obtained by the quasi-2$^{\text{nd}}$-order scheme. Again it can be seen that the amplitude of the oscillations are intensified as the moment order increases. It is worth mentioning that employing the standard 2^{nd}-order TVD scheme is not feasible because the moments get corrupted shortly after starting the simulation and consequently the Chebyshev algorithm fails to calculate the weights and the abscissas required for the source calculation. Even reducing the time step by a factor of 100, equivalent to an impractically small CFL value of 0.005, cannot remedy the non-realizability problem. This shows the effectiveness of the proposed equal-limiter scheme in preserving the realizability of the moments when the 2^{nd}-order TVD schemes are employed.

Symmetric constant breakage kernel. In this case, the source term in Eq. (7) is calculated as follows [23]:

$$h_i^k = \sum_{\alpha=1}^{3} w_{i,\alpha} 2^{(3-k)/3} L_{i,\alpha}^k K_b - \sum_{\alpha=1}^{3} w_{i,\alpha} L_{i,\alpha}^k K_b \tag{53}$$

where $K_b = 4\ (s^{-1})$ is the breakage kernel.

Fig. 4 depicts the results provided by the studied schemes along with the analytical solutions. The same arguments presented for the case of pure aggregation apply also to this case with the difference that here the oscillating behavior of the quasi 2^{nd}-order scheme is more intense. This further highlights the advantage of the equal-limiter scheme whenever the boundedness of the solution is strictly required.

5.2. Pure advection in two-dimensional transient flow

The previous part presents satisfactory results obtained by the equal-limiter scheme in the one-dimensional constant-velocity Riemann problem examples. However, it is important to examine the predictions obtainable by the proposed scheme in systems with higher dimensions and realistic flow fields, e.g. non-constant and/or transient velocity. For this purpose, a familiar two-dimensional transient flow, known as lid-driven cavity, is selected to compare the results for the pure advection of moments obtained by employing upwind, quasi-2$^{\mathrm{nd}}$-order and equal-limiter schemes. The moments belong to the distributions that represent the population of micro-droplets which are transported by a carrier liquid. The micro-droplets are assumed to do not have their own inertia and therefore they move with the same velocity of the carrier liquid.

The simulation domain is a square with length (L) of 10 cm and it is discretized by a structured uniform Cartesian grid comprising of 10000 square cells of size 1 mm. The flow is confined by four boundaries of type wall, from which the top one moves with the velocity (U) of 1 (m/s) while the others are fixed. The kinematic viscosity of the liquid (ν) is set to 2.5×10^{-4} (m^2/s), which results to Reynolds number of 400 defined by UL/ν. The liquid is assumed to be stagnant at time zero and then a transient flow develops in the liquid due to the constant velocity (U) applied at the top wall.

The transient simulations are done by using the icoFoam solver of OpenFOAM software, which solves the governing (constant-density) Navier-Stokes equations for the liquid phase numerically by using the PISO algorithm [16]. The time step is set to 0.0001 (s) to keep the maximum Courant number below 0.1. The solution of the velocity field at three time instants are shown in Fig. 5. The solver is modified to solve simultaneously the moment transport equations. At the beginning of each time step, the moments of the micro-droplet population are advected in time using the velocity field of the previous time step. Then, the flow field of the liquid phase is updated by using the PISO algorithm. Regarding the advection of moments, as mentioned in Section 4, the implicit Euler time-integration can be used with the advection schemes that deal with the moments directly, and therefore is adopted here when the upwind and equal-limiter schemes are employed. On the other hand, the quasi-2$^{\text{nd}}$-order scheme is implemented with Euler explicit time-integration. It should be noted that the reasoning behind employing the implicit time-integration scheme is to highlight the advantage of the equal-limiter scheme, which is its compatibility with the implicit approach. Concerning the flux-limiter, the minmod function is used for the interpolation of quadrature weights in case of employing quasi-2$^{\text{nd}}$-order scheme and the interpolation of moments in case of employing equal-limiter scheme.

Two different cases corresponding to two different initial conditions for the moments are considered. The first initial condition is defined such that there is no micro-droplets in the domain except for a square patch where a population of micro droplets with average size of 100 (μm) and standard deviation of 20 (μm) is introduced. The population is assumed to be distributed log-normally on the size space. The initial conditions for the moments are calculated based on this log-normal distribution which is scaled to adjust the volume fraction of the micro-droplets equal to 0.05 (assuming spherical shape for the micro-droplets). Fig. 6 depicts the initial conditions for the moment of order three, along with the solutions for the same moment at $t = 3$ s obtained by employing the 1$^{\text{st}}$-order upwind, quasi-2$^{\text{nd}}$-order and equal-limiter schemes. As can be seen, the solution obtained by the upwind scheme suffers from high numerical diffusion. On the other hand, both the quasi-2$^{\text{nd}}$-order and equal-limiter schemes yield comparable results, which have higher resolution with respect to the one obtained by the upwind scheme. It is noteworthy that the same contour plots (but of different values) are obtained for the other moments, which is expected since the shape of the distribution corresponding to the underlying NDF remains the same in pure advection. As a result, the abscissas of the quadrature approximation are the same in all the cells of the domain.

As mentioned previously, the quasi-2$^{\text{nd}}$-order scheme interpolates the quadrature abscissas with a 1$^{\text{st}}$-order scheme, whereas it interpolates the quadrature weights with a 2$^{\text{nd}}$-order scheme. Therefore, when the quadrature abscissas are the same throughout the domain, the entire resolution of the quasi-2$^{\text{nd}}$-order scheme for the pure advection of moments is the same as the 2$^{\text{nd}}$-order scheme. The reason is that, in this case, the value of abscissas on the faces are the same as those at the cell centers regardless of the employed scheme. Consequently, the pure advection of moments by interpolating the weights onto the faces with a given 2$^{\text{nd}}$-order scheme and then constructing the moments on the faces (using the same abscissas) is equivalent to the pure advection of moments by interpolating the moments directly onto the faces using that 2$^{\text{nd}}$-order scheme. However, this equivalency is not generally valid when the abscissas are not the same through the domain. Thus, it is worth examining the performance of the schemes in case of existing two different distributions, i.e. having different quadrature abscissas, in the system at time zero. For this purpose, the same square patch (with the same population of micro-droplets) defined by the initial conditions of the previous case is considered also here. However, it is assumed that another population of micro-droplet exists outside the square patch, instead of assuming no micro-droplet existing in that zone. Let the population of micro-droplets out of the square patch be also distributed log-normally on the size space with average size equal to 50 (μm) and standard deviation of 7.5 (μm). This distribution is scaled to have the volume fraction of the micro-droplets equal to 0.001. Then, the initial condition of the moments is defined based on this scaled distribution, as shown in Figs. 7 and 8 for the moments of order zero and three respectively. Moreover, the predictions at $t = 3$ s are depicted by these figures for the mentioned moments. As can be seen in Fig. 7, the values of M_0 obtained by employing the quasi-2$^{\text{nd}}$-order scheme do not remain bounded between the limits defined by the initial conditions. It is noteworthy that in QBMM, the transported variables are indeed the moments and therefore in the pure advection with a solenoidal velocity field, the solution for the moments should remain bounded between the limits defined by the initial conditions. This issue concerning the quasi-2$^{\text{nd}}$-order scheme can be associated to the fact that this scheme interpolates the weights and abscissas of the quadrature separately, and therefore there is no guarantee that the TVD criteria [20] are respected by this scheme. On the other hand, the solution obtained by the equal-limiter scheme (when it is used with the minimum limiter) respects the boundedness property of the moments. Moreover, the applied change in the initial condition of the moments should not change the pattern of the solution contour plots, since the current initial condition with the two distributions can be changed to a problem with initial condition similar to the previous case (micro droplets existing only in a square patches) by a change of variables. However, the comparison between the results shown in Fig. 8 with those depicted in Fig. 6 highlights that only the equal-limiter scheme reproduces the same pattern for M_3 in both cases. Furthermore, the pattern of the results obtained by the equal-limiter scheme for M_0 and M_3 shown in Figs. 7 and 8 are the same, whereas this is not the case for the results obtained by the quasi-2$^{\mathrm{nd}}$-order scheme. This final example emphasizes the advantage of employing a scheme which interpolates the moments directly, e.g. equal-limiter scheme, instead of interpolating some variables related to the moments.

6. Conclusions

A new technique called equal-limiter scheme was proposed to overcome the non-realizability problem that arises when the 2$^{\mathrm{nd}}$-order TVD schemes are employed to solve the moment transport equations in the context of QBMM. The central idea behind the technique is that the interpolated moments on the faces must form a realizable set when the moment fluxes are being calculated. Following this idea, it was explained that using an identical flux-limiter for all the moments at each face guarantees the realizability of the interpolated moments and consequently helps to preserve the realizability of the transported moments. Although no formal proof has been given to ensure that the equal-limiter scheme preserves the realizability of the moments under general conditions, it has been shown that this feature can be achieved in the limit of small time steps (as long as the moment sets are far from the boundary of the moment space). On the contrary, adjusting the time step can not mitigate the non-realizability problem if the limiters are independently calculated for each moment of the transported moment set. This fact was also illustrated by the numerical tests as the moments did not remain realizable even with impractically small time step in the case of employing the standard 2nd-order TVD scheme. Moreover, it was proved that the minimum limiter is a possible practical option for the equal limiter if the boundedness feature of the TVD schemes has to be retained. Although selecting the minimum limiter may imply solutions of lower order, the one-dimensional numerical examples showed that the results obtained by equal-limiter and quasi-2nd-order schemes are comparable in terms of accuracy. More importantly, the improvement in the accuracy was observed also for the solutions obtained by the equal-limiter scheme in a one-way coupled QMOM-CFD simulation of a transient two-dimensional flow. Furthermore, the new technique does not only improve the accuracy of the solution with respect to the 1st-order solution but also keeps the solution bounded, which was shown to be an advantage over the quasi-2nd-order scheme by comparing their predictions in both one- and two-dimensional numerical examples. In addition, the implementation of the scheme is simple and can be integrated into the CFD simulations easily.

The future works will focus on applying the proposed scheme to the three-dimensional CFD simulation of polydisperse systems and studying its predictions in comparison to those of the other discretization schemes.

References

[1] D. L. Marchisio, R. O. Fox, Computational Models for Polydisperse Particulate and Multiphase Systems, Cambridge Series in Chemical Engineering, Cambridge University Press, Cambridge, UK, 2013.

[2] R. G. Gordon, Error bounds in equilibrium statistical mechanics, Journal of Mathematical Physics 9 (1968) 655–663.

[3] J. C. Wheeler, Modified moments and Gaussian quadratures, Rocky Mountain Journal of Mathematics 4 (1974) 287–296.

[4] O. Desjardins, R. O. Fox, P. Villedieu, A quadrature-based moment method for dilute fluid-particle flows, Journal of Computational Physics 227 (2008) 2514–2539.

[5] D. L. Wright Jr., Numerical advection of moments of the particle size distribution in Eulerian models, Journal of Aerosol Science 38 (2007) 352–369.

[6] V. Vikas, Z. J. Wang, A. Passalacqua, R. O. Fox, Realizable high-order finite-volume schemes for quadrature-based moment methods, Journal of Computational Physics 230 (2011) 5328–5352.

[7] A. Buffo, M. Vanni, D. L. Marchisio, On the implementation of moment transport equations in openfoam: boundedness and realizability, International Journal of Multiphase Flow 85 (2016) 223–235.

[8] D. Kah, F. Laurent, M. Massot, S. Jay, A high order moment method

simulating evaporation and advection of a polydisperse liquid spray, Journal of Computational Physics 231 (2) (2012) 394–422.

[9] F. Laurent, T. T. Nguyen, Realizable second-order finite-volume schemes for the advection of moment sets of the particle size distribution, Journal of Computational Physics 337 (2017) 309–338.

[10] C. Berthon, et al., Stability of the MUSCL schemes for the Euler equations, Communications in Mathematical Sciences 3 (2) (2005) 133–157.

[11] D. Ramkrishna, Population Balances: Theory and Applications to Particulate Systems in Engineering, 1st Edition, Academic Press, 2000.

[12] D. L. Marchisio, R. O. Fox, Solution of population balance equations using the direct quadrature method of moments, Journal of Aerosol Science 36 (2005) 43–73.

[13] J. A. Shohat, J. D. Tamarkin, The problem of moments, American Mathematical Society, New York, USA, 1943.

[14] M. Pigou, J. Morchain, P. Fede, M.-I. Penet, G. Laronze, New developments of the extended quadrature method of moments to solve population balance equations, Journal of Computational Physics 365 (2018) 243–268.

[15] R. J. LeVeque, Finite Volume Methods for Hyperbolic Problems, 1st Edition, Cambridge University Press, 2002.

[16] J. H. Ferziger, M. Peric, Computational Methods for Fluid Dynamics, 3rd Edition, Springer, Berlin, Germany, 2001.

[17] P. Roe, M. Baines, Algorithms for advection and shock problems, in: Numerical Methods in Fluid Mechanics, 1982, pp. 281–290.

[18] B. Van Leer, Towards the ultimate conservative difference scheme. II. monotonicity and conservation combined in a second-order scheme, Journal of computational physics 14 (4) (1974) 361–370.

[19] C. Yuan, R. O. Fox, Conditional quadrature method of moments for kinetic equations, Journal of Computational Physics 230 (2011) 8216–8246.

[20] A. Harten, High resolution schemes for hyperbolic conservation laws, Journal of computational physics 49 (3) (1983) 357–393.

[21] P. K. Sweby, High resolution schemes using flux limiters for hyperbolic conservation laws, SIAM journal on numerical analysis 21 (5) (1984) 995–1011.

[22] H. K. Versteeg, W. Malalasekera, An Introduction to Computational Fluid Dynamics: The Finite Volume Method, 2nd Edition, Pearson Education, 2007.

[23] D. L. Marchisio, R. D. Vigil, R. O. Fox, Quadrature method of moments for aggregation-breakage processes, Journal of Colloid and Interface Science 258 (2003) 322–334.

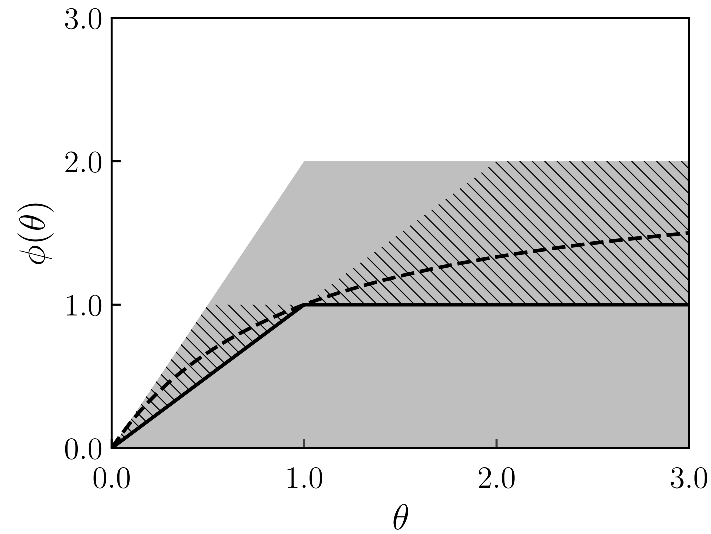

Figure 1: Flux-limiter functions. The shaded area specifies the TVD region and the hatched area is the 2$^{\text{nd}}$-order region by Sweby [21]. The minmod [17] and van Leer [18] limiter functions are shown by the continuous and dashed curves respectively.

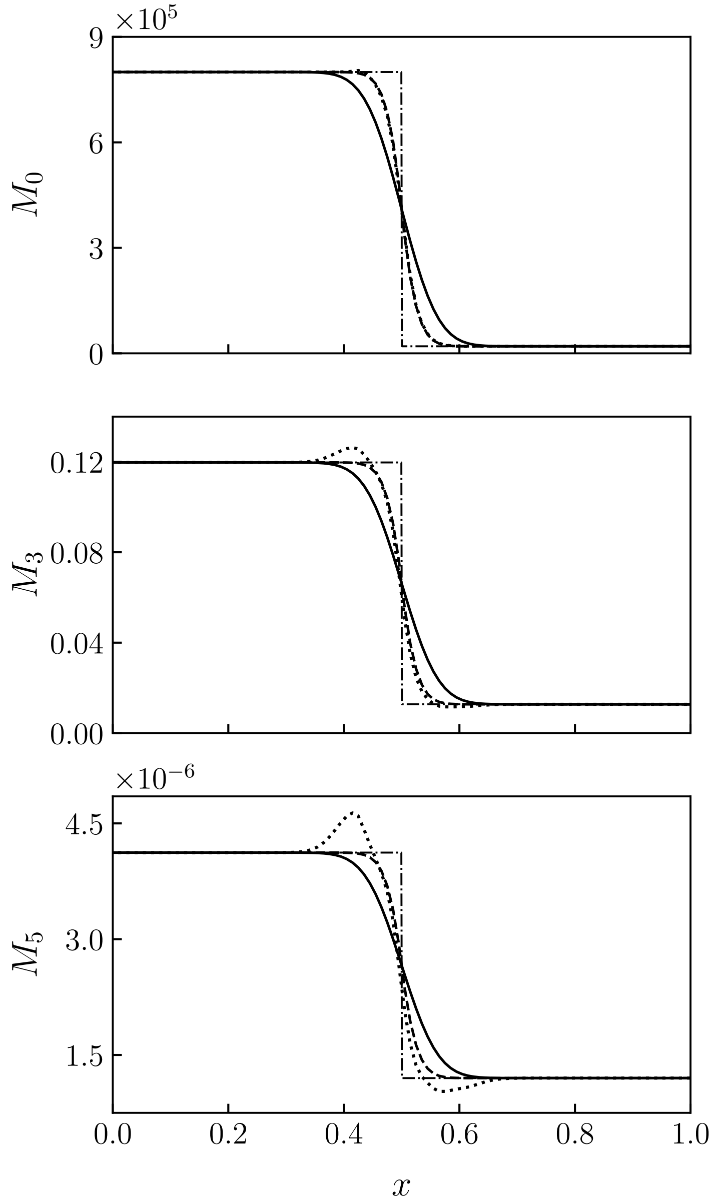

Figure 2: Comparison of the results obtained by employing different schemes for the case of pure advection: 1) analytical solution (dot-dashed line); 2) upwind scheme (continuous line); 3) quasi 2^{nd}-order scheme (dotted line); 4) equal-limiter scheme (dashed line)

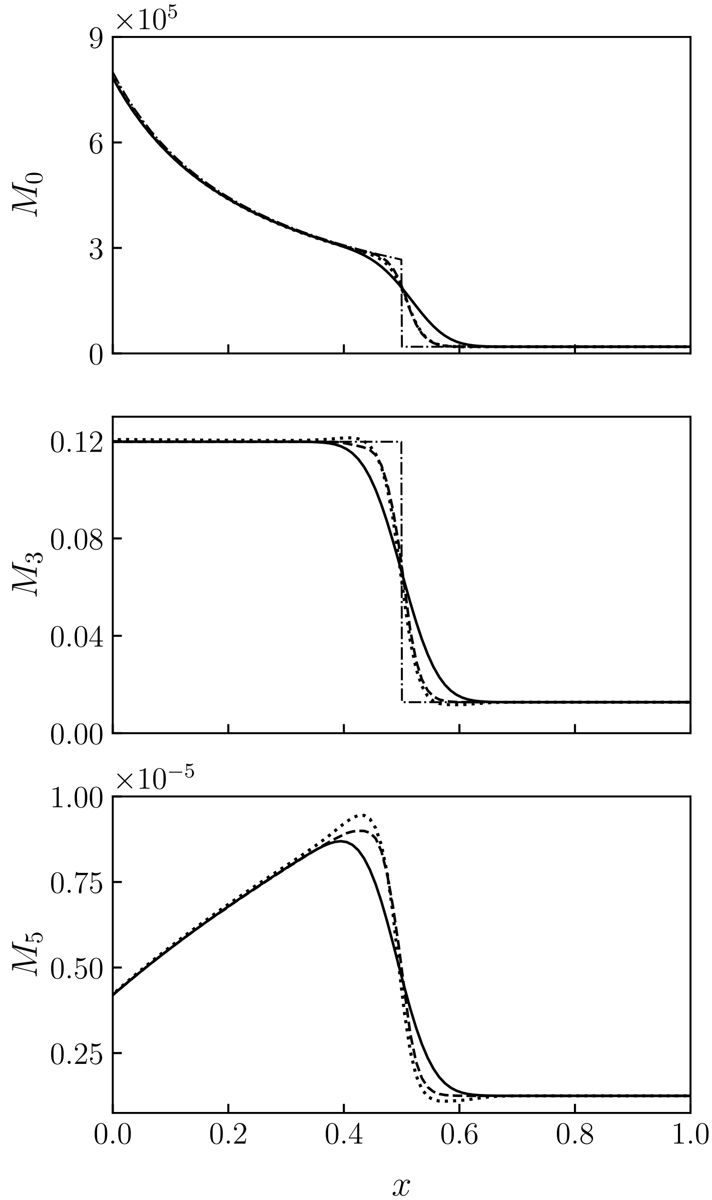

Figure 3: Comparison of the results obtained by employing different schemes for the case of constant aggregation kernel: 1) analytical solution if available (dot-dashed line); 2) upwind scheme (continuous line); 3) quasi 2$^{\text{nd}}$-order scheme (dotted line); 4) equal-limiter scheme (dashed line)

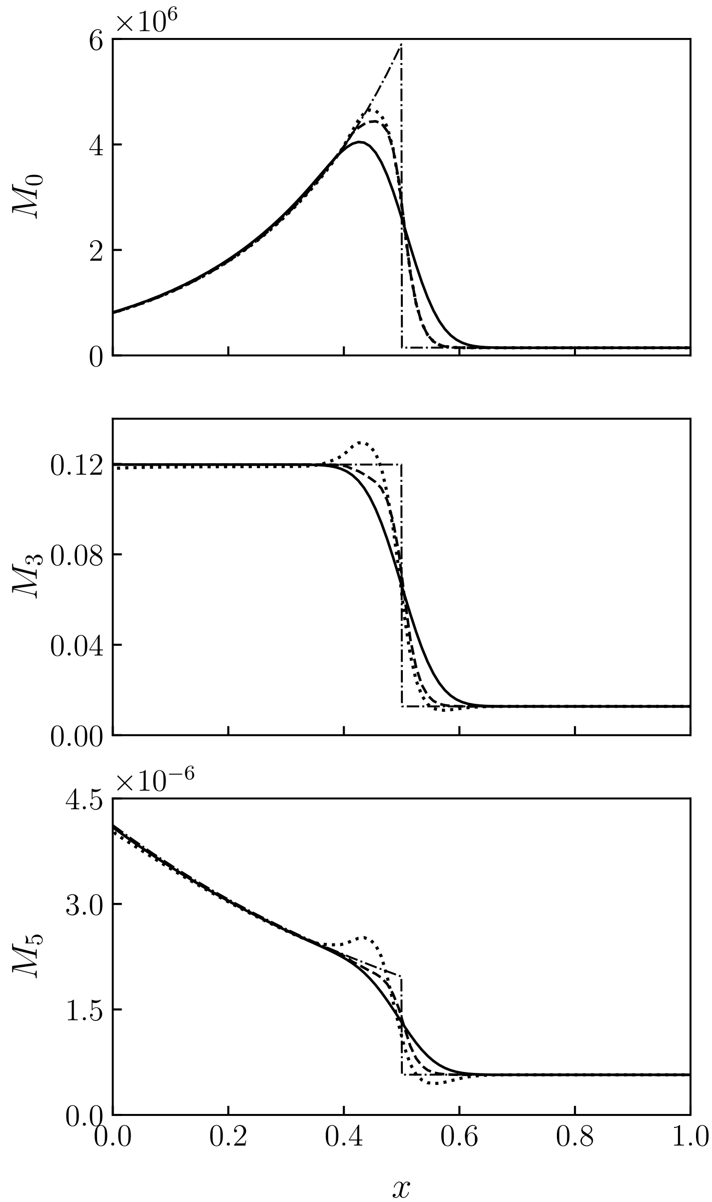

Figure 4: Comparison of the results obtained by employing different schemes for the case of symmetric constant breakage kernel: 1) analytical solution (dot-dashed line); 2) upwind scheme (continuous line); 3) quasi 2^{nd}-order scheme (dotted line); 4) equal-limiter scheme (dashed line)

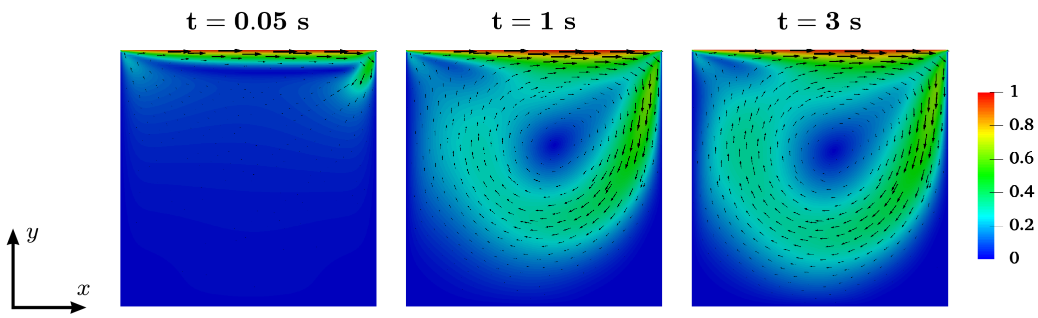

Figure 5: Velocity field (m/s) of the simulated 2-D lid-driven cavity flow at three time instants.

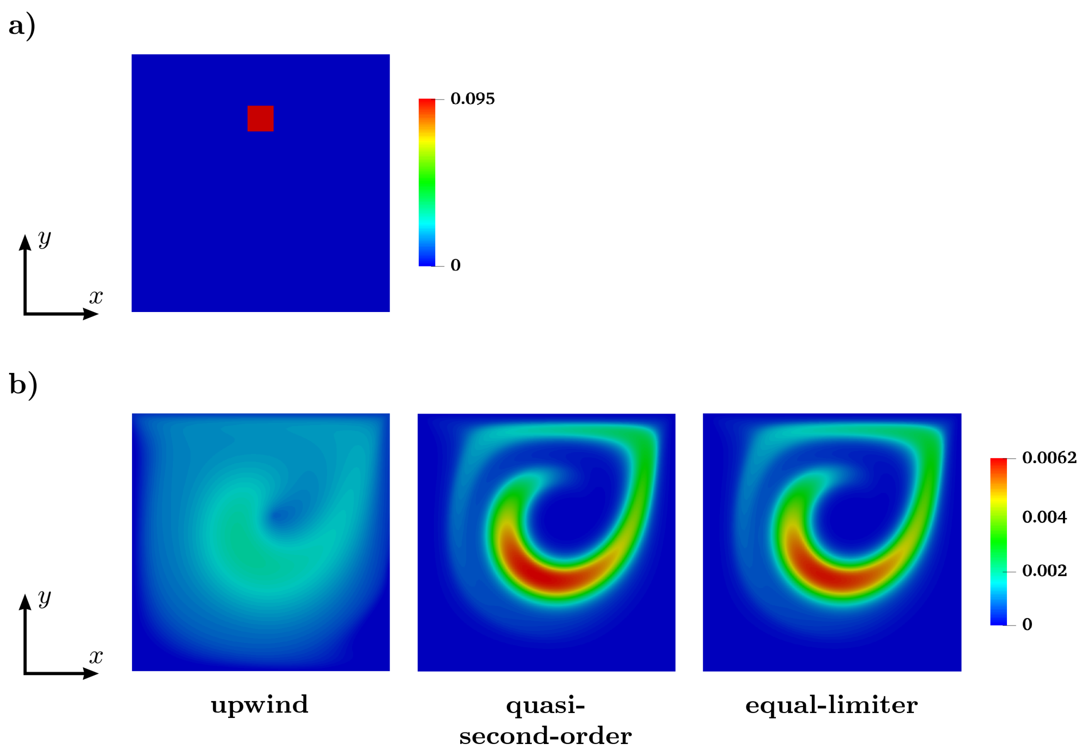

Figure 6: Comparison of the studied schemes for the advection of M_3 in the 2-D cavity flow. (a) The initial condition at $t = 0$; (b) the predictions obtained by employing the different schemes at $t = 3$.

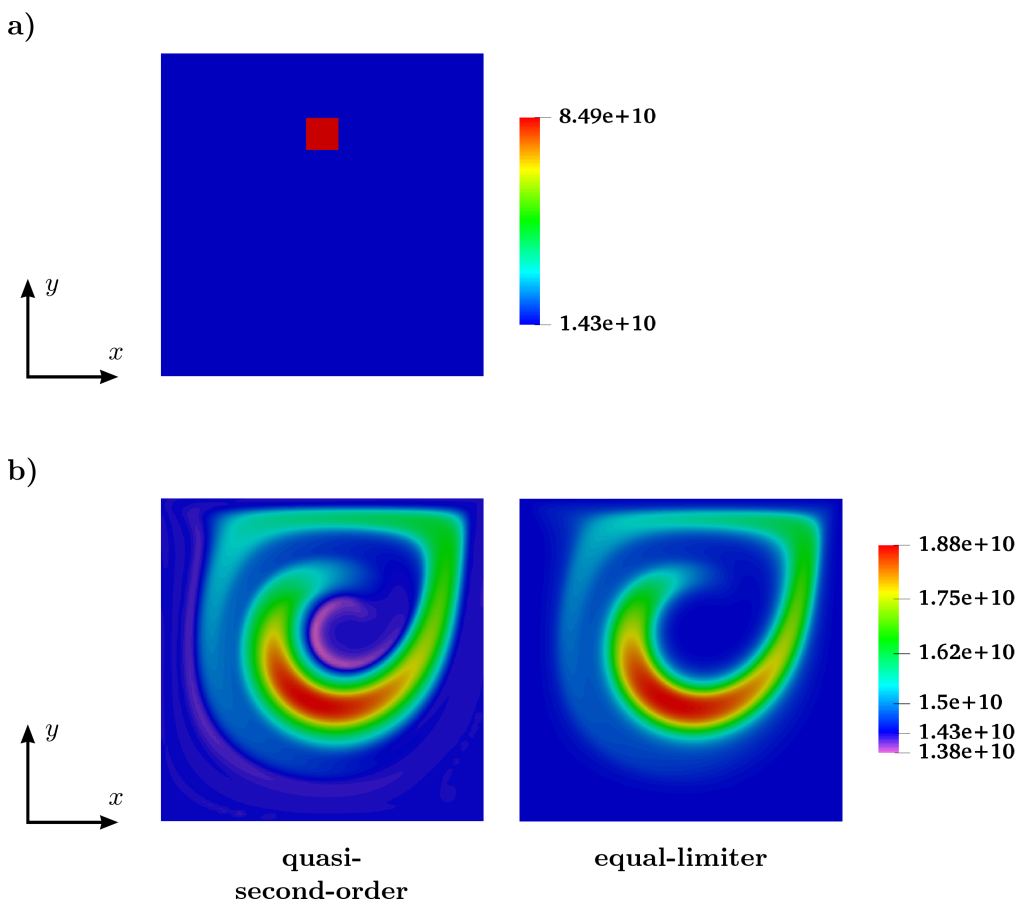

Figure 7: Comparison of the studied schemes for the advection of M_0 in the 2-D cavity flow in case of existing two different distributions in the domain. (a) The initial condition at $t = 0$; (b) the predictions obtained by employing the different schemes at $t = 3$.

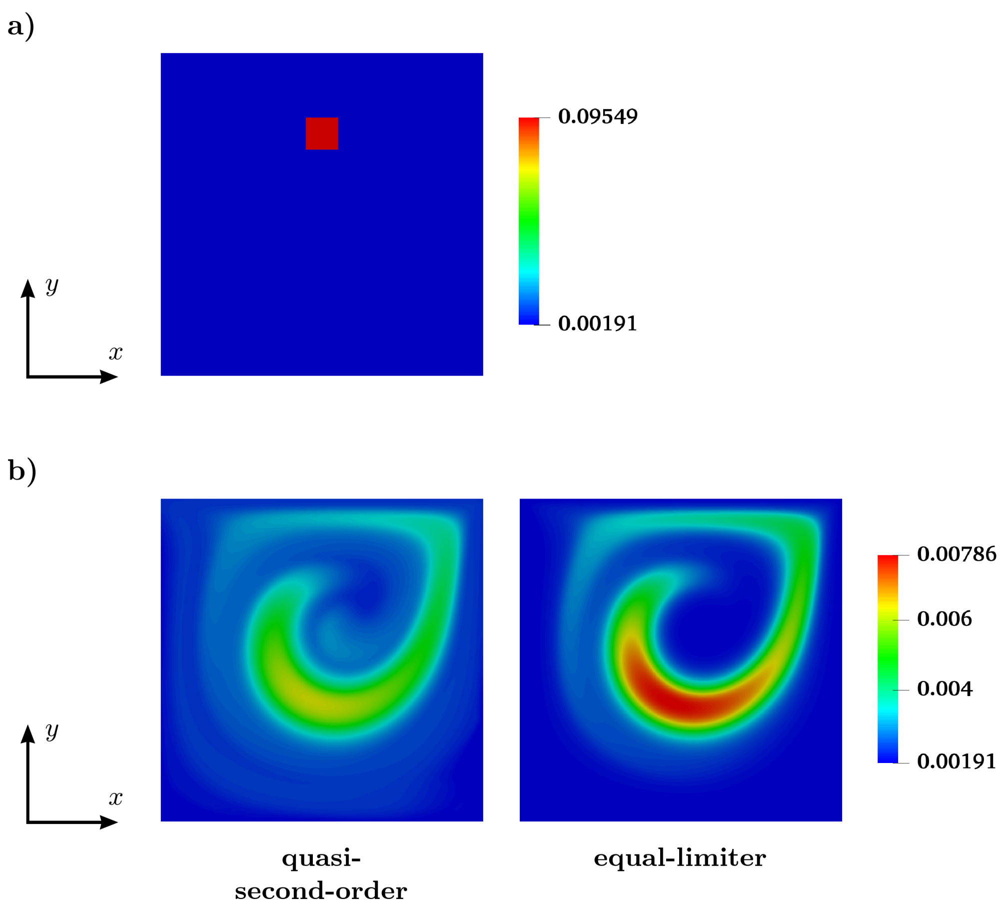

Figure 8: comparison of the studied schemes for the advection of M_3 in the 2-D cavity flow in case of existing two different distributions in the domain. (a) The initial condition at $t = 0$; (b) the predictions obtained by employing the different schemes at $t = 3$.